

Article

Synthesis of Magnesium-Based Alloys by Mechanical Alloying for Implant Applications

Sergio Gonzaga¹, Arturo Molina^{2,*} , René Guardián², Horacio Martínez¹, Edna Vázquez Vélez¹ 
and Jesús Santa-Olalla Tapia³ 

¹ Instituto de Ciencias Físicas, Universidad Nacional Autónoma de México, Av. Universidad 1000, Col. Chamilpa, Cuernavaca 62210, Morelos, México

² Centro de Investigación en Ingeniería y Ciencias Aplicadas (IICBA), Universidad Autónoma del Estado de Morelos, Cuernavaca 62209, Morelos, México

³ Departamento de Fisiología y Farmacología, Facultad de Medicina, Universidad Autónoma del Estado de Morelos, Calle Leñeros s/n, Col. Los Volcanes, Cuernavaca 62350, Morelos, México

* Correspondence: arturo_molina@uaem.mx

Abstract: The biocompatibility and biodegradability of magnesium (Mg), along with its lightness, make magnesium-based materials promising for use in the biomedical industry. In this work, ternary Mg–Zn–Ca alloys were manufactured for biomedical applications using mechanical alloying (MA). The objective of this work was to study the effect of milling time on the produced ternary alloys Mg65–Zn30–Ca5 and Mg70–Zn25–Ca5 (percentages by weight), the degradation of the alloys in synthetic human fluids, and their generated cytotoxicity. The Mg-based alloys were synthesized in a planetary ball mill under an argon atmosphere using stainless-steel containers and balls with a milling regimen of 400 rpm for 2, 5, 10, 15, and 20 h. The powders obtained after MA were characterized by scanning electron microscopy (SEM) and X-ray diffraction (XRD), which verified that ternary Mg–Zn–Ca alloys can be obtained using MA. The XRD refinement analysis of the samples showed the presence of a MgZn intermetallic phase. Electrochemical tests showed that the corrosion resistance and corrosion current density of Mg65–Zn30–Ca5 and Mg70–Zn25–Ca5 alloys improved compared to those of pure Mg. Cytotoxicity testing was conducted using the Sulforhodamine B (SRB) assay, which revealed that the alloys did not exhibit cytotoxicity toward human fibroblast cells. Mg65–Zn30–Ca5 and Mg70–Zn25–Ca5 alloys show good potential to be used in biomedical applications.

Keywords: biomaterials; mechanical alloying; magnesium alloys



Citation: Gonzaga, S.; Molina, A.; Guardián, R.; Martínez, H.; Vélez, E.V.; Tapia, J.S.-O. Synthesis of Magnesium-Based Alloys by Mechanical Alloying for Implant Applications. *Coatings* **2023**, *13*, 260. <https://doi.org/10.3390/coatings13020260>

Academic Editor: Petric® Vizureanu

Received: 17 November 2022

Revised: 6 January 2023

Accepted: 19 January 2023

Published: 22 January 2023



Copyright: © 2023 by the authors. Licensee MDPI, Basel, Switzerland. This article is an open access article distributed under the terms and conditions of the Creative Commons Attribution (CC BY) license (<https://creativecommons.org/licenses/by/4.0/>).

1. Introduction

Magnesium (Mg) alloys can function as temporary implants owing to their light weight, together with their elastic modulus and compressive strength comparable with those of human bone [1,2]. The density of bone is 1.8–2.1 g/cm³, which is almost equal to that of Mg (1.738 g/cm³), while the elastic modulus of natural bone is 40–57 GPa, which is like that of Mg (45 GPa) [3]. Natural Mg is a cofactor for several enzymes and makes stable RNA and DNA structures [4,5]. In addition, it is biodegradable and biocompatible in body fluids, thus reducing the need for the removal of the temporary implant because Mg alloys can degrade slowly in physiological conditions without producing toxicity. Further, in vitro, in vivo, and clinical studies suggested that Mg-based implants show good biocompatibility [4]. Thus, Mg alloys can be considered as degradable, load-bearing orthopedic implants that can maintain their mechanical properties during bone tissue repair for over 12–18 weeks [2,6]. However, the use of Mg alloys is not recommended because only a limited number of elements (Zn and Ca) that meet the biocompatibility requirements exists [7,8]. Zn is a vital ingredient [9] implicated in numerous characteristics of cellular metabolism. It is necessary for the catalytic action of around 100 enzymes [10], cell division, and protein and DNA synthesis [11]. Approximately 99% of the Ca in the human

body is deposited in teeth and bones [12]. Ca is vital for sustaining the potential difference through excitable cell membranes, as well as for correct bone structure [13,14]. Zinc has been added to Mg alloys to increase corrosion resistance, while Ca has been added to induce mineralization [15,16]. Most commercial Mg alloys contain Al, which is known to induce neurotoxicity [17], and rare earth elements, which cause severe hepatotoxicity [18]. Mg–Zn–Ca alloys were formed using machine-driven alloying (MA) given that it is an efficient way to yield alloys with a fine microstructure, which promotes greater mechanical properties [19,20], MA is an exclusive solid-state reaction process that happens between the surfaces of fine particles at room temperature; consequently, MA can be used to create alloys difficult or impossible to obtain using conventional systems. Thus, the MA method has inspired numerous investigations. Nevertheless, there is little evidence accessible on the production of Mg alloys made with the MA procedure; hence, more investigation is required to generate Mg-based alloys with the required properties for temporary implant treatments. In this study, magnesium-based biomaterials were synthesized using MA with the following compositions: Mg₆₅–Zn₃₀–Ca₅ and Mg₇₀–Zn₂₅–Ca₅ (wt.%). These compositions were based on the criteria established by different authors and studies that have been carried out [21–23]. In addition, the elements Zn and Ca definitely effect bone remediation, cell viability, stability in physiological environments, cellular reactions, and cell proliferation, and when alloyed together Mg–Zn–Ca give important benefits to absorbable polymers since alloys are easier to sterilize and do not liberate acid products [24]. The X-ray diffraction (XRD) analysis of the tests showed the existence of a MgZn intermetallic phase. Vickers microhardness (Hv) tests were conducted by applying an indentation load of 200 g. Cytotoxicity assessment was performed using primary human fibroblast cells for Mg, Mg₆₅–Zn₃₀–Ca₅, and Mg₇₀–Zn₂₅–Ca₅. The objective of this paper was to explore the development and characterization of Mg-based alloys using MA. These results may be useful in processing biodegradable and biocompatible alloys with controlled corrosion without eliciting any toxic response under physiological conditions. The results further demonstrate that Mg-based alloys can display excellent mechanical properties while aiding bone regeneration as temporary implants.

2. Materials and Methods

Mixtures of Mg (99.5%), Zn (99.7%), and Ca (99.8%) powders were mechanically alloyed with a composition of Mg₆₅–Zn₃₀–Ca₅ and Mg₇₀–Zn₂₅–Ca₅ (wt.%), utilizing times of 2, 5, 10, 15, and 20 h with a rate of 400 rpm. The MA method was conducted employing a low-energy Fritsch Pulverisette planetary mill in an argon atmosphere. The ball-to-powder weight proportion of 10:1 was maintained constant through the milling procedure by employing stainless-steel balls with a 10 mm diameter. Weighed and encapsulated powders in an argon atmosphere were used to begin the MA procedure. XRD and scanning electronic microscopy (SEM, Cambridge, Ltd. Cambridge, England) were employed to analyze the powders. A scanning electron microscope with a voltage of 20 kV, equipped with energy-dispersive spectroscopy (EDS), was used to determine the morphology of the obtained powders. The final milled powders were pressed using cold isostatic pressing at 400 MPa for 5 min. The compacted powders were sintered at 400 °C for 4 h in an argon atmosphere.

A typical three-electrode system (ACM Instruments, Cumbria, UK) consisting of a graphite rod as a counter electrode, a platinum electrode as a reference electrode, and samples of Mg, Mg₆₅–Zn₃₀–Ca₅, and Mg₇₀–Zn₂₅–Ca₅ (0.5-inch diameter) as working electrodes was used to perform potentiodynamic polarization tests in Hank's solution [25] at 37 °C. Potentiodynamic polarization experiments were performed at a scan rate of 0.5 mV/s. The samples were polished with 2000-grit SiC paper, rinsed with distilled water, and dried. The corrosion potentials (E_{corr}) and corrosion current densities (I_{corr}) of the samples were estimated from the Tafel extrapolations of polarization curves.

Cytotoxicity tests were performed via indirect contact with primary human fibroblast cells (ATCC PCS-201-010). Fibroblast cells were cultured in Dulbecco's modified Eagle's medium, supplemented with 10% fetal bovine serum (FBS), 100 U/μL of penicillin,

0.25 $\mu\text{g}/\mu\text{L}$ of fungizone, and 2 mM GlutaMAX (ThermoFisher) in a 5% CO_2 incubator. The sintered samples were polished with SiC papers (from 400 to 2000 grit), ultrasonically cleaned with ethanol for 7 min, sterilized with ultraviolet light for 30 min on both sides, and placed in 15 mL falcon tubes at 25 $^\circ\text{C}$. For the preparation of the extracts, the previously sterilized samples were incubated with the fibroblast culture medium for 24 h in an atmosphere with 5% CO_2 at 37 $^\circ\text{C}$, according to ISO 10,993-12 [26]. The extract was centrifuged to remove the degraded material. Then, the supernatant was aspirated and stored in a refrigerator at 4 $^\circ\text{C}$ before cytotoxicity testing. The extract concentration was diluted to 100%, 75%, 50%, and 25%. Then, four samples of each extract were placed separately in 96-well cell culture plates (1×10^4 cells/200 μL medium) and the cells were incubated for 96 h to allow cell proliferation. The morphology of the cell growth was then observed using light microscopy and the fibroblast cell viability was evaluated applying the SRB (Sigma-Aldrich, Darmstadt, Germany) test [27]. In an SRB assay, a bright pink aminoxanthene dye shapes an electrostatic complex with the amino acid residue of proteins in slightly acidic environments; thus, the assay determines the total biomass of the cells. SRB has been widely applied to establish the toxicity of drugs and different materials on cancerous and non-cancerous cells [28,29]. The relative cell growth rates (RGRs) were calculated using Equation (1):

$$\text{RGR} = (\text{Experimental Group OD Mean} / \text{Negative Control Group OD Mean} \times 100\%) \quad (1)$$

Cell viability is a cytotoxicity detection technique that gives information about the biocompatibility of a material. The SRB assay is a conventional and effective method for detecting cell viability. Furthermore, this test is one of the innovative colorimetric cell-based assays. The quantity of the SRB dye obtained from the stained cells is directly proportional to the total protein mass and, thus, links to the living cell numbers [30,31].

3. Results

Morphologies and particle sizes of the elemental powders are displayed in Figure 1. The SEM micrographs exhibit a mainly flake-like morphology for Mg, a spherical shape for Zn, and an irregular morphology for Ca (Table 1).

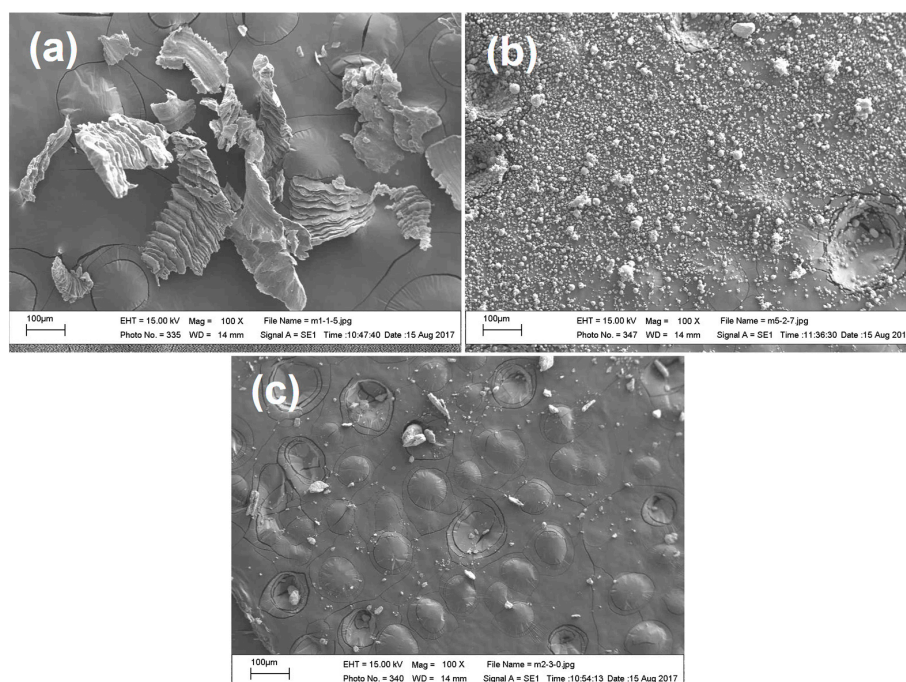


Figure 1. Initial powders of (a) Mg, (b) Zn, and (c) Ca. Reprinted from Ref. [25]. Physics SRL, 2021.

Table 1. Initial powder size and morphology.

Initial Powders	Average Particle Size (μm)	Morphology
Mg	30	Flake-like
Zn	5	Spherical
Ca	20	Irregular

During grinding, a very fine mixture of the components is formed. This mixture is most often lamellar in the case of ductile metal powders. Obtaining the alloy itself is mediated by the defects at the level of a crystalline lattice (dislocations, stacking faults, vacancies, etc.) formed as a result of severe cold plastic deformation. These defects facilitate rapid diffusion while also leading to a slight increase in powder temperature during milling due to frictional forces and the impact between the milling balls and the surface of the container. Suryanarayana [32] also explained that the necessary energy is obtained to reach a homogeneous microstructure of powder particles with the same composition as the proportion of the constituent powders because of the repeated severe plastic deformations of the powder particles, which are cold-welded and constantly fractured afterward. Figures 2 and 3 display the particle size and morphology variation as the milling time increases for the Mg65–Zn30–Ca5 and Mg70–Zn25–Ca5 powder mixtures, respectively. The SEM micrographs (Figures 2 and 3) of the Mg65–Zn30–Ca5 and Mg70–Zn25–Ca5 powder mixtures after 15 h of milling displayed two types of distortion mechanisms characteristic of the MA process that happened during milling: ductile deformation, which forms flatter and longer particles linked to the deformation experienced by Mg during the first hours of milling, and brittle deformation, which results in the creation of particles with a more angular and irregular morphology typical of brittle materials. Ductile deformation, which results in the formation of larger particles, has been reported by Abdoli [33]. The powder mixtures subjected to 15 and 20 h of milling (Figures 2 and 3) showed that the particle size decreased compared with the samples milled for 15 h. In addition, the particle shape became irregular, indicating that the brittle fracture was predominant because of the hardening due to the deformation exhibited in both compositions.

The quantitative elemental analyses of Mg65–Zn30–Ca5 and Mg70–Zn25–Ca5 milled for 20 h indicated the presence of Mg, Zn, and Ca (Figure 4). The EDS results revealed that the weight percentages of Mg, Zn, and Ca were, respectively, $65.54 \pm 1.23\%$, $29.32 \pm 4.32\%$, and $5.13 \pm 3.11\%$ in Mg65–Zn30–Ca5 and $71.68 \pm 2.97\%$, $25.32 \pm 4.13\%$, and $2.74 \pm 3.01\%$ in Mg70–Zn25–Ca5 (Table 2).

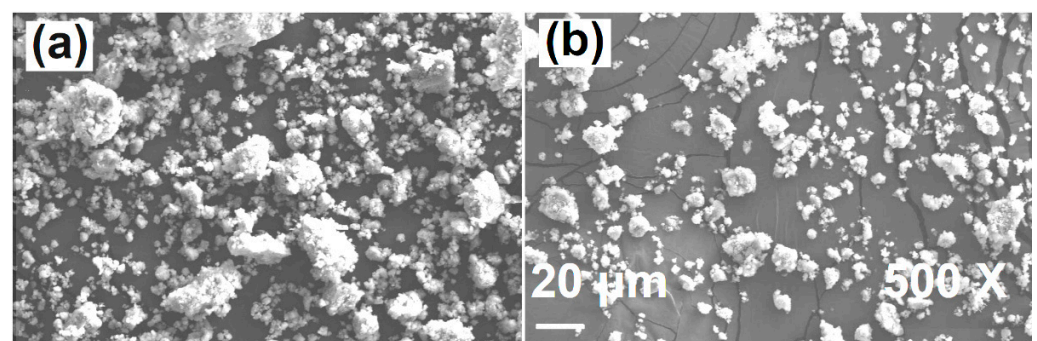


Figure 2. SEM micrographs of Mg65–Zn30–Ca5 milled for (a) 15 and (b) 20 h. Reprinted from Ref. [25]. Physics SRL, 2021.

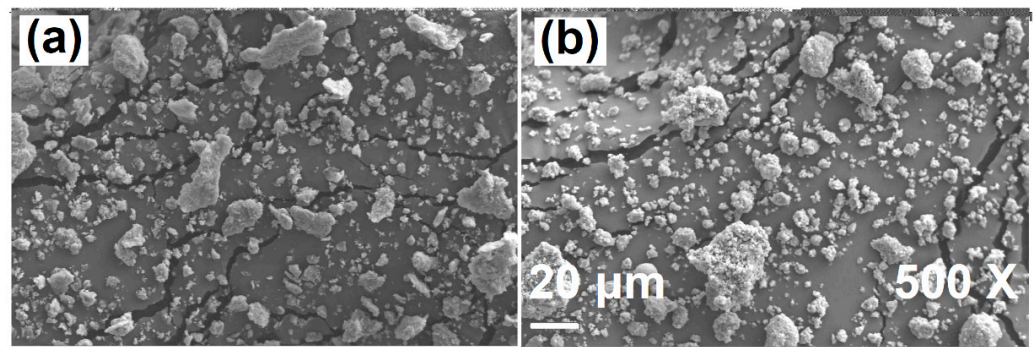


Figure 3. SEM micrographs of Mg70–Zn25–Ca5 milled for (a) 15 and (b) 20 h. Reprinted from Ref. [25]. Physics SRL, 2021.

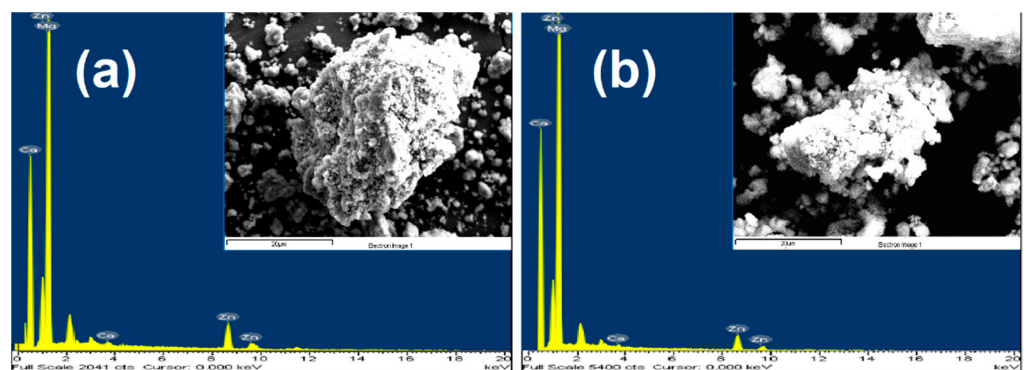


Figure 4. SEM-EDS micrographs of (a) Mg65–Zn30–Ca5 and (b) Mg70–Zn25–Ca5 milled for 20 h.

Table 2. Quantitative elemental analyses (wt.%) of Mg65–Zn30–Ca5 and M70–Zn25–Ca5 milled for 20 h, measured using SEM-EDS.

Composition	(wt. %)		
	Mg	Zn	Ca
Mg65–Zn30–Ca5	65.54 ± 1.23	29.32 ± 4.33	5.13 ± 3.11
Mg70–Zn25–Ca5	71.68 ± 2.97	25.32 ± 4.13	2.74 ± 3.01

Figure 5a shows the evolution of particle size as the milling time progressed for Mg65–Zn30–Ca5. After 2 h of milling, the particle size was in the range of 5–14 μm, and after 20 h of milling, the average particle size was between 2 μm and 6 μm. For Mg70–Zn25–Ca5 (Figure 5b), after 2 h of milling, the average particle size was in the range of 11–16 μm, and after 20 h, the average particle size decreased, varying in the range of 3–5 μm.

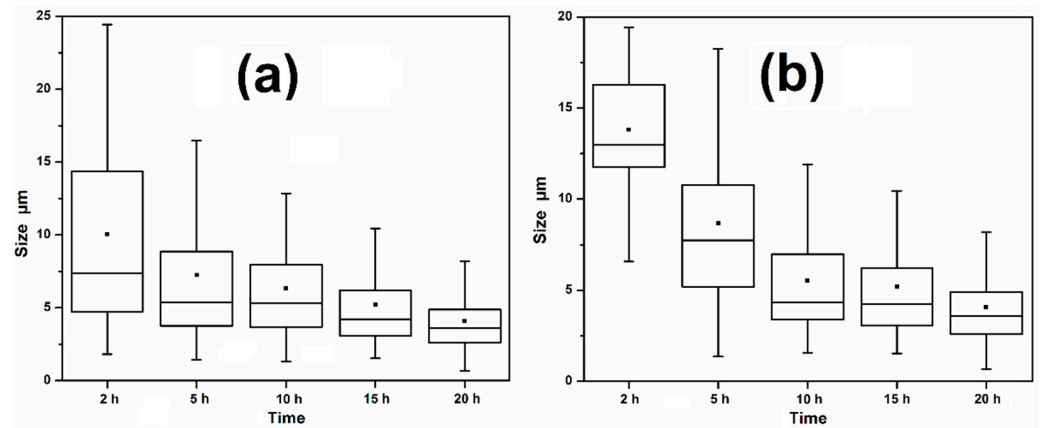


Figure 5. Particle size evolution of (a) Mg₆₅–Zn₃₀–Ca₅ and (b) Mg₇₀–Zn₂₅–Ca₅ when mechanically alloyed for milling times of 2, 5, 10, 15, and 20 h.

3.1. XRD Analysis

XRD patterns (Figures 6 and 7) at various milling times display a reduction in peak intensity and flattening. This behavior may be related to the amorphization activity of the alloy. The amorphization process in ordered alloy systems seems to obey the following sequence [34]:

Ordered phase → *Disordered* → *Crystallite size reduction* → *Amorphous phase*

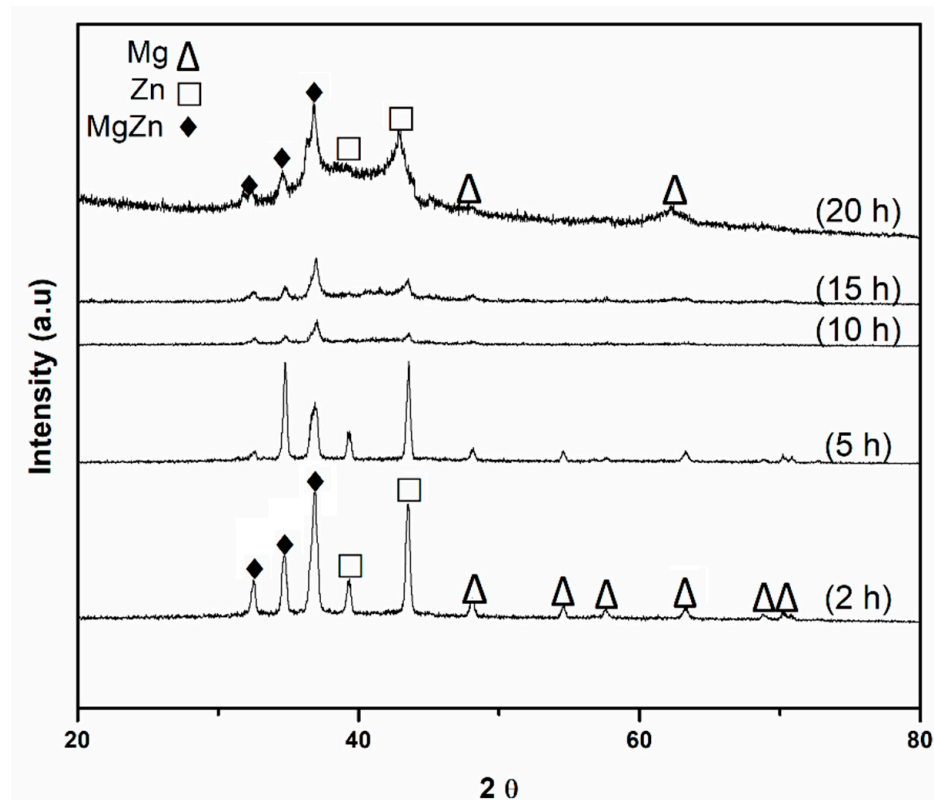


Figure 6. XRD patterns of Mg₆₅–Zn₃₀–Ca₅ mechanically alloyed for milling times of 2, 5, 10, 15, and 20 h.

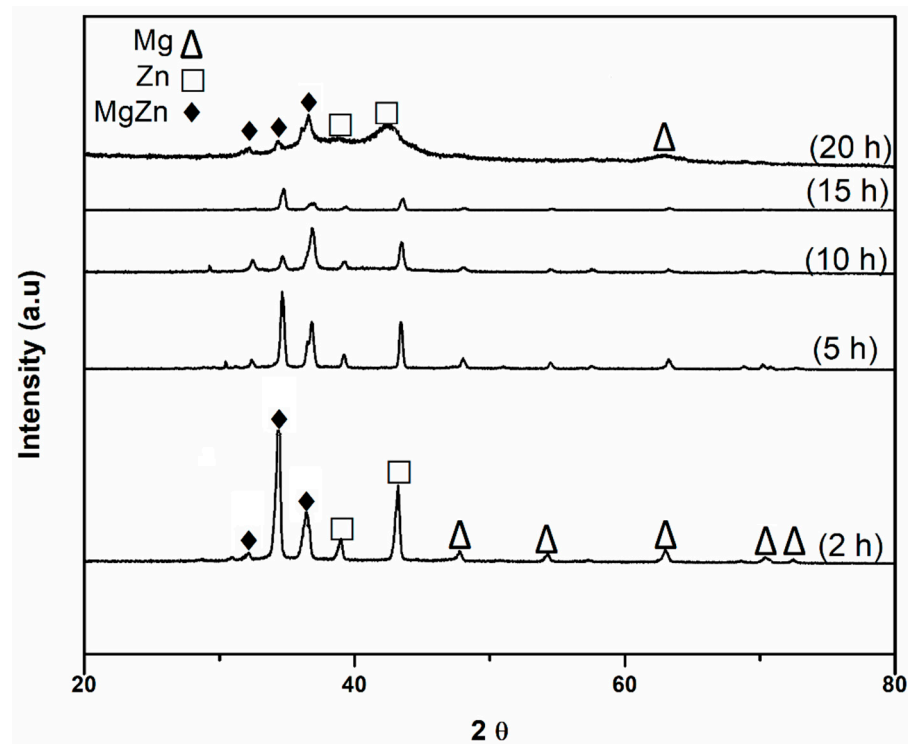


Figure 7. XRD patterns of Mg₇₀–Zn₂₅–Ca₅ mechanically alloyed for milling times of 2, 5, 10, 15, and 20 h.

The XRD patterns for the milling time of 20 h displayed the existence of a MgZn intermetallic phase in both alloying systems. This result suggests that Mg, Zn, and Ca form a homogeneous mixture after up to 15 h of milling without any diffusive reaction occurring between the elements. Table 3 shows the elements, types of phases, and angles found in the XRD analyses. Together with XRD analysis, SEM-EDS analyses were performed to verify the obtained chemical compositions after the MA process (Table 2). The results indicated that the applied MA parameters allowed us to obtain the initially proposed chemical compositions.

Table 3. Angles in the XRD patterns (Figure 7) and their corresponding phases.

Symbol	Angle (2 θ)	Element or Phase (Chemical Composition)
Δ	47.76	Mg
Δ	54.30	Mg
Δ	57.30	Mg
Δ	63.00	Mg
Δ	68.55	Mg
Δ	69.92	Mg
□	39.33	Zn
□	43.21	Zn
◆	32.05	MgZn
◆	34.74	MgZn
◆	37.12	MgZn

3.2. Sintering

Various composite materials have been produced using MA, and nanocomposites of amorphous phases have also been found, which crystallized at relatively low temperatures [35]. The XRD patterns of the sintered Mg₆₅–Zn₃₀–Ca₅ and Mg₇₀–Zn₂₅–Ca₅ and the powders subjected to 20 h of milling are shown in Figures 8 and 9. The diffraction

peaks grew after sintering. This behavior may be linked with the crystallization of Mg, Zn, and Ca owing to the sintering process.

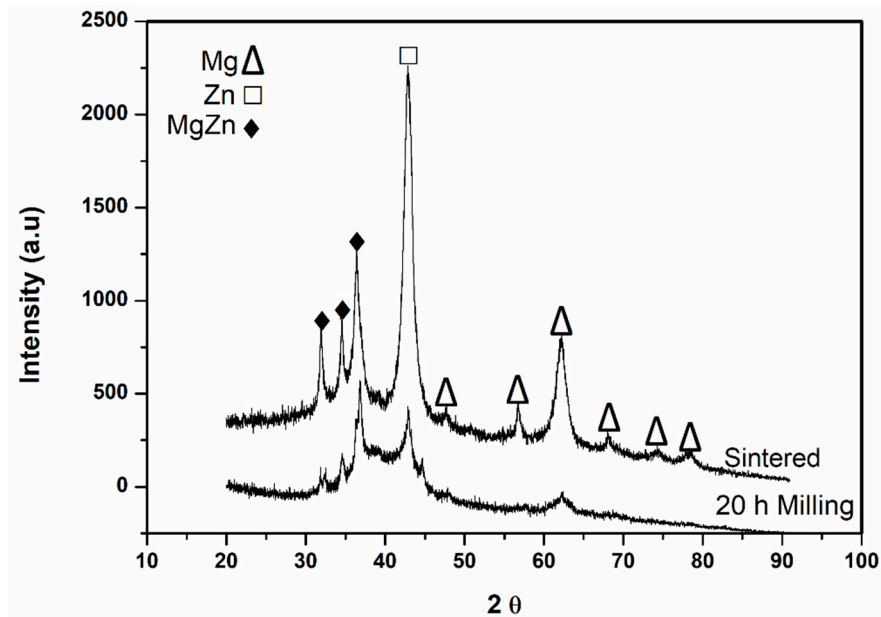


Figure 8. XRD patterns of the Mg65–Zn30–Ca5 obtained and the powders milled for 20 h.

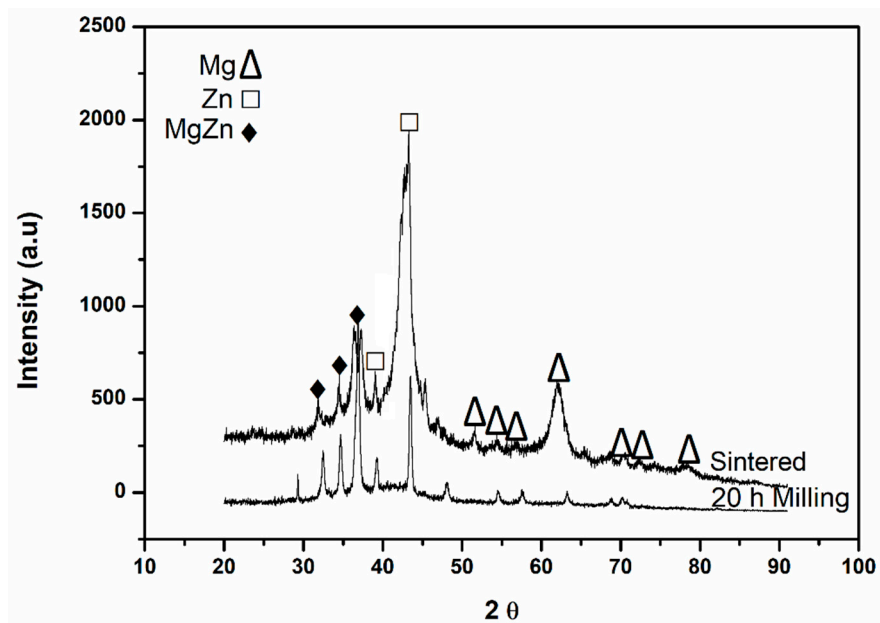


Figure 9. XRD patterns of the Mg70–Zn25–Ca5 obtained and the powders milled for 20 h.

3.3. Electrochemical Polarization Curves

A promising application of Mg alloys is the previously developed absorbable stent [36], which has been successfully tested for implanting. For orthopedic biomaterials, 3–4 months are needed [37] for the development of fibroblasts and chondroblasts in the fracture zone for new bone generation and, finally, the consolidation of solid bone restoring most of the original bone strength [38]. Thus, Mg-alloy-based orthopedic implants must maintain their mechanical properties for at least 3 months to avoid the occurrence of fractures. Potentiodynamic corrosion measurements were conducted using a characteristic three-electrode system, which consisted of a graphite rod as the counter electrode, a platinum electrode as the reference electrode, and half-inch-diameter samples as the working elec-

trode. The E_{corr} (corrosion potential), I_{corr} (corrosion current density) and corrosion rate (CR) of the sintered samples of Mg, Mg65–Zn30–Ca5, and Mg70–Zn25–Ca5 are shown in Table 4. The corrosion potentials of Mg65–Zn30–Ca5 (–1374.45 mV) and Mg70–Zn25–Ca5 (–1311.61 mV) were considerably higher than that of Mg (–1456.81). The corrosion rate of the alloys was calculated using the corrosion current density [39]. The calculated corrosion rates were approximately 0.277 mm/year for the magnesium, 0.191 mm/year for the Mg65Zn30Ca alloy, and 0.218 mm/year for the Mg70Zn25Ca5 alloy. These results indicated that the corrosion resistance of Mg was improved by adding Zn as an alloying element. The lower corrosion current density indicates better corrosion resistance and a lower corrosion rate. It can be deduced from the above results that Mg65–Zn30–Ca5 and Mg70–Zn25–Ca5 alloys show better corrosion resistance and lower corrosion rates compared to Mg (Figure 10) due to the addition of Zn, which improved the corrosion potentials of the alloys. Increasing the corrosion rate with the addition of Zn can be due to the formation of galvanic couples between Zn particles as the anode and the Mg matrix as the cathode, which further accelerates the corrosion process [40].

Table 4. E_{corr} , I_{corr} , and corrosion rate of Mg, Mg65–Zn30–Ca5, and Mg70–Zn25–Ca5.

Sample	E_{corr} (mV)	I_{corr} (mA/cm ²)	CR (mm/year)
Mg	–1456.81	5.93×10^{-1}	0.277
Mg65–Zn30–Ca5	–1374.45	4.02×10^{-1}	0.191
Mg70–Zn25–Ca5	–1311.61	4.54×10^{-1}	0.218

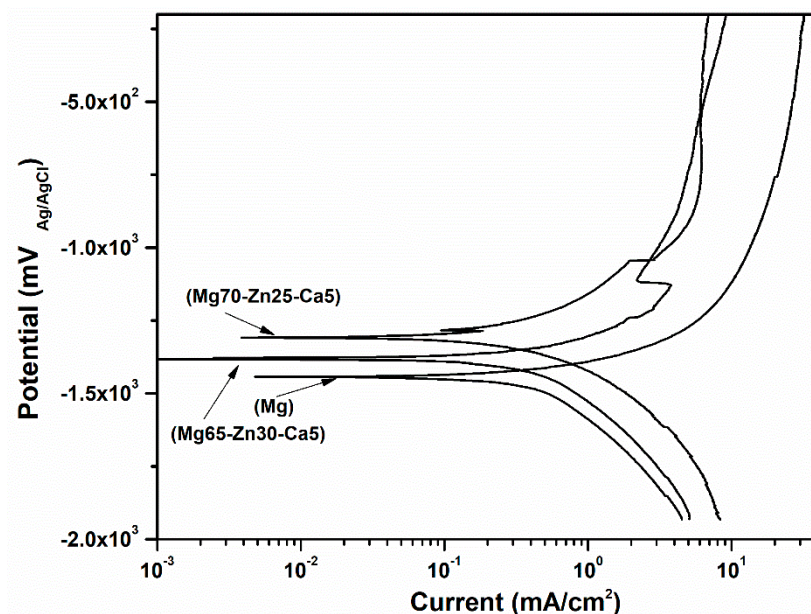


Figure 10. Potentiodynamic polarization curves of Mg, Mg65–Zn30–Ca5, and Mg70–Zn25–Ca5.

The scanning electron micrographs showed the corrosion products formed at the surfaces of Mg, Mg65–Zn30–Ca5, and Mg70–Zn25–Ca5 (Figure 11) during potentiodynamic polarization tests. The EDS results (Figure 12) showed that the corrosion products consisted of O, Mg, Zn, Ca, Cl, P, and Na elements. Due to the composition of Hank's solution, it is very difficult to recognize the compositions of the corrosion products; however, the elements detected after EDS indicated the formation of MgO and MgCl₂.

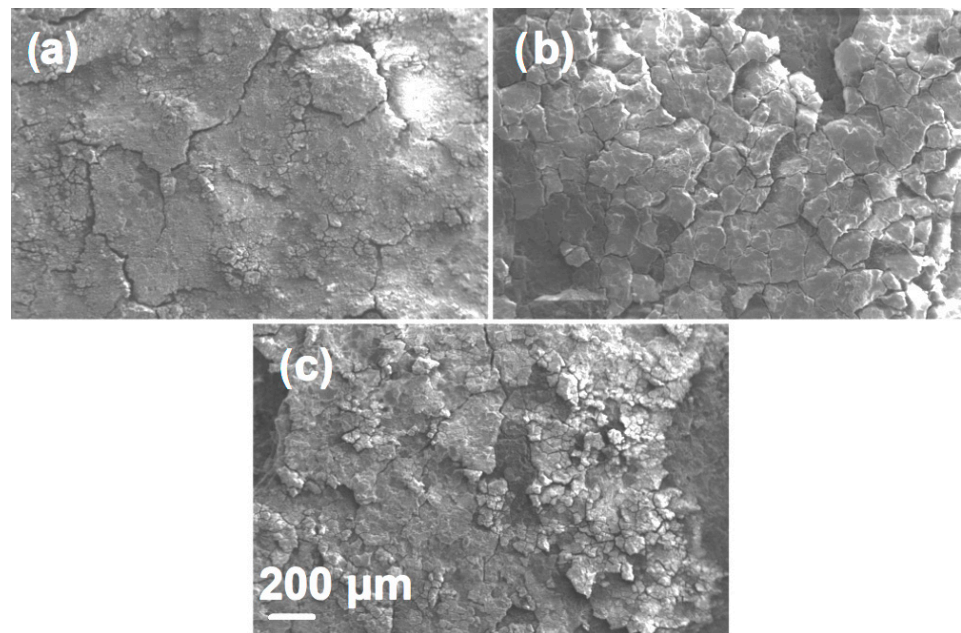


Figure 11. SEM micrographs of (a) Mg, (b) Mg65–Zn30–Ca5, and (c) Mg70–Zn25–Ca5 after potentiodynamic polarization tests.

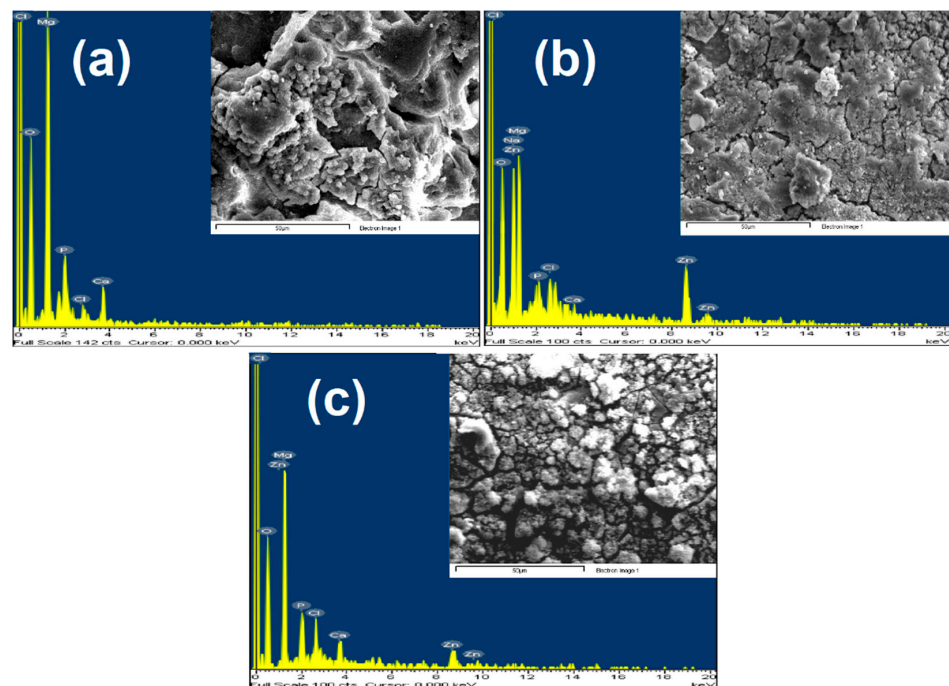


Figure 12. SEM-EDS micrographs of (a) Mg, (b) Mg65–Zn30–Ca5, and (c) Mg70–Zn25–Ca5 after potentiodynamic polarization tests.

3.4. Cytotoxicity Test

The results of the cytotoxicity tests showed good fibroblast cell proliferation in different concentrations of the extracts of Mg, Mg65–Zn30–Ca5, and Mg70–Zn25–Ca5. The RGR results are shown in Figure 13. For extract concentrations of 100%, 75%, 50%, and 25%, the RGRs of pure Mg were 71%, 84%, 76%, and 90%; the RGRs of Mg65–Zn30–Ca5 were 98%, 91%, 89%, and 93%; and the RGRs of Mg70–Zn25–Ca5 were 99%, 83%, 99%, and 97%. The results obtained for the alloys Mg65–Zn30–Ca5 and Mg70–Zn25–Ca5 suggest that they are not toxic to human cells, so they can be used for biomedical applications.

Figure 14 shows the morphology and proliferation of fibroblasts after 96 h of incubation in different concentrations of the extracts.

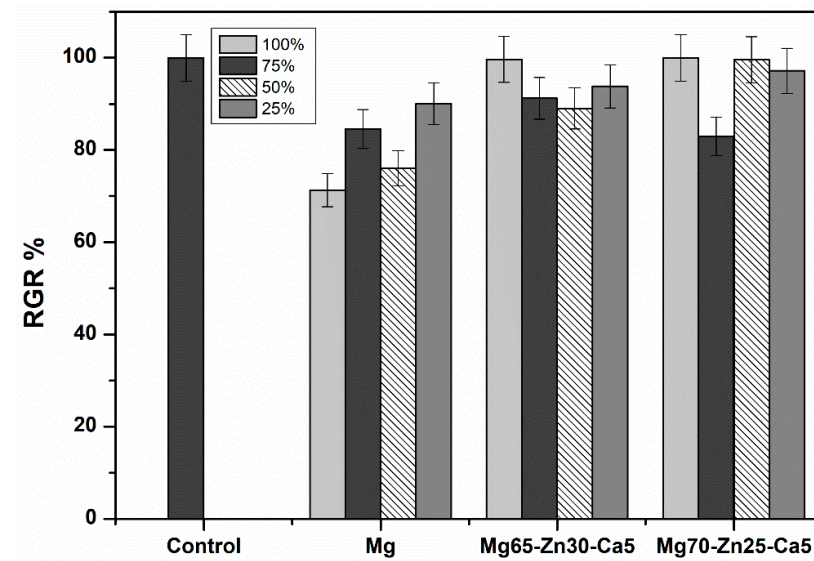


Figure 13. Cytotoxicity test results.

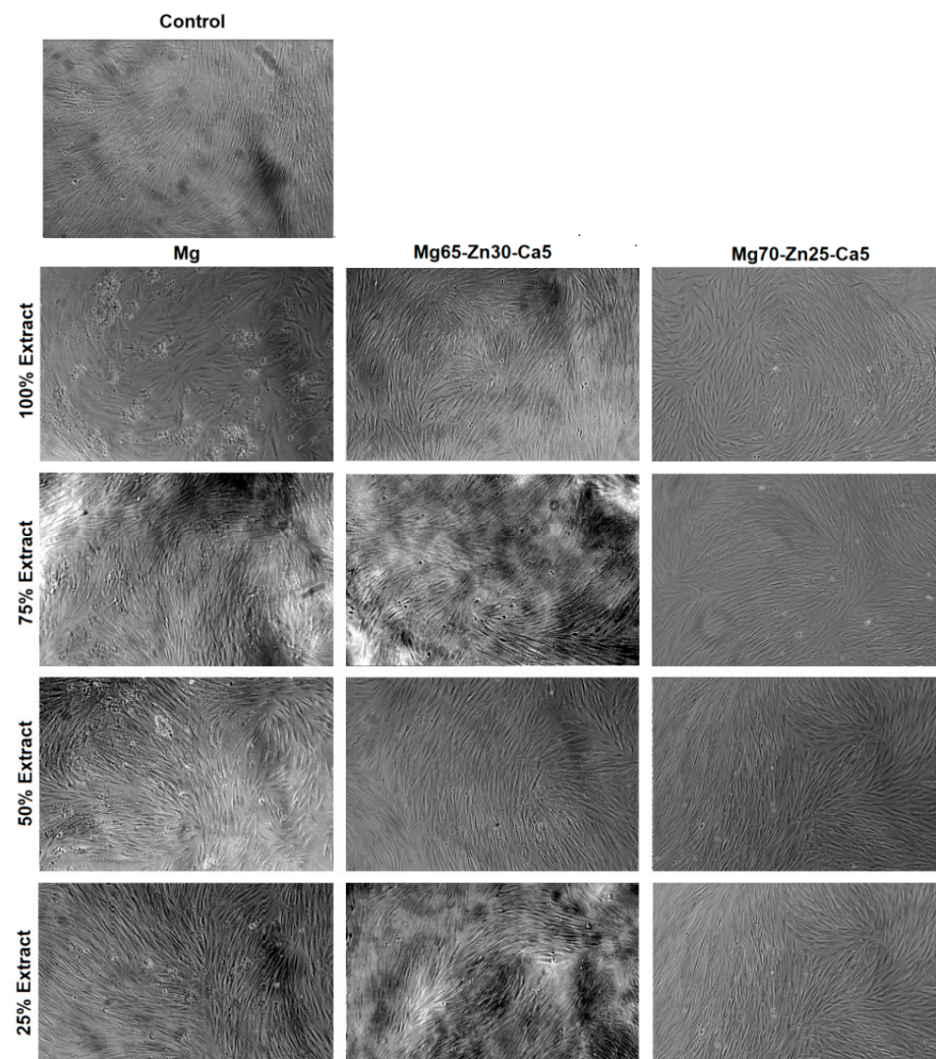


Figure 14. Morphology and proliferation of cultured fibroblasts after 96 h (enhanced contrast).

3.5. Microhardness Test

The implantation of biomaterials such as bone plates and stents is used to replace human tissues; thus, they must possess mechanical properties comparable to those of the replaced tissues [1,15,41,42]. Mg alloys can exhibit a wide range of tensile strength (from 86.8 to 280 MPa) and elongation (from 3% to 21.8%) values. A study showed that the addition of Al, Ag, In, Si, Sn, and Zr can improve both the strength and elongation of Mg alloys [1] and that their effects can be improved by a posterior process, such as hot rolling or hot extrusion [1,15,43].

The microhardnesses of the sintered samples are shown in Table 5. The microhardnesses of pure Mg, Mg65–Zn30–Ca5, and Mg70–Zn25–Ca5 were 52.7 ± 8 Hv, 72.8 ± 4 Hv, and 79.9 ± 3 Hv. The increase in the microhardness values of the alloys was ascribed to the work hardening mechanism that happened due to severe plastic deformation through uniaxial consolidation. Additionally, as the milling time grew, the dispersion of Zn and Ca particles in the Mg matrix was more homogeneous, resulting in stronger bonding between the reinforcement and the matrix.

Table 5. Microhardness test.

Specimen	Vickers Microhardness (Hv)
Mg	52.70 ± 8
Mg65–Zn30–Ca5	72.80 ± 4
Mg70–Zn25–Ca5	79.90 ± 3

4. Discussion

Figures 2 and 3 show that, after 5 h of milling, the Mg65–Zn30–Ca5 and Mg70–Zn25–Ca5 powders experienced ductile deformation, so large conglomerates were formed. This is consistent with the study by Suryanarayana [44] on ductile–brittle systems. In Mg65–Zn30–Ca5 and Mg70–Zn25–Ca5, it can be seen that after 15 h of milling, there was a decrease in the amount of larger conglomerates due to the cold work hardening phenomenon of the MA process, which causes the fracture of particles to be more dominant than cold welding at the late stage of milling due to the particles being hardened by mechanical work, which leads to the fragmentation of the particles. The alloys subjected to different milling times showed that the particle size decreased in relation to milling time. The data obtained from the powders after EDS (Table 3) indicated that the Mg, Zn, and Ca percentages were, respectively, $65.54 \pm 1.23\%$, $29.32 \pm 4.32\%$, and $5.13 \pm 3.11\%$ for Mg65–Zn30–Ca5 and $71.68 \pm 2.97\%$, $25.32 \pm 4.13\%$, and $2.74 \pm 3.01\%$ for Mg70–Zn25–Ca5, which promoted the formation of the MgZn intermetallic phase. The EDS analysis was carried out in a timely manner on the particles, with which the composition varies slightly from particle to particle; however, the average of a group of particles is close to the elemental composition initially proposed and the results obtained show the presence of the items used. XRD was used to investigate the existing phases in the Mg65–Zn30–Ca5 and Mg70–Zn25–Ca5 alloys, as displayed in Figures 6 and 7. The MgZn phase was produced in both alloys. The XRD and EDS analysis carried out in this work did not show the presence of Fe impurities or any type of foreign element. In the same way, it should be noted that the process was carried out in the cleanest way possible to avoid the contamination of the samples. In addition, the MA process uses a low-energy planetary ball mill which is used in laboratory tests. The potentiodynamic polarization curves of Mg65–Zn30–Ca5 and Mg70–Zn25–Ca5 alloys in Hank's solution are shown in Figure 10. As shown in Figure 10, the corrosion potentials of Mg65–Zn30–Ca5 and Mg70–Zn25–Ca5 alloys were higher than that of pure Mg. The corrosion potential was correlated with the Zn content. In physiological conditions, the presence of dissolved oxygen, chloride, and sodium in the blood, carbon dioxide and water content in the tissues, and cellular metabolism have direct impacts on the degradation of Mg alloys in vivo [45,46]. For example, in the EDS results obtained after conducting polarization tests in Hank's solution, O, Mg, Zn, Ca, P, Cl, and Na were detected (Figure 12). The

results of the cellular cytotoxicity investigated using the indirect SRB assay (Figure 13) revealed that at different concentrations of the extracts, negligible cytotoxicity was observed. Additionally, Figure 14 shows cell morphologies in different extracts, indicating that they were healthy, which is similar to that of the control. The concentration of contaminants of Fe or other elements is very low; therefore, it is not expected to have any influence on cytotoxicity. From the preliminary results of the two alloys synthesized in this work, the alloy that can be proposed for temporary implantation is Mg70–Zn25–Ca5 since it presents better microhardness (Hv) and electrochemical properties. In the same way, it is intended to carry out more studies on these alloys. Owing to the properties of the synthesized alloys, they can be applied as filling materials for bone deficiencies and temporary orthopedic implants for broken phalanges or other small bones.

5. Conclusions

The Mg-based alloys Mg65–Zn30–Ca5 and Mg70–Zn25–Ca5 (wt.%) were successfully synthesized from pure Mg, Zn, and Ca powders after applying the MA procedure. The XRD patterns indicated the creation of a MgZn intermetallic phase through the MA process. The results acquired from XRD and SEM analyses suggest that it is feasible to synthesize Mg65–Zn30–Ca5 and Mg70–Zn25–Ca5 alloys using MA by applying a low-energy regime. Potentiodynamic polarization curves showed that pure Mg had a lower corrosion resistance compared to Mg65–Zn30–Ca5 and Mg70–Zn25–Ca5 alloys, showing that the increased Zn content can help to form a protective film on the alloy surface and increase corrosion resistance. The cell viability tests obtained via the indirect SRB assay showed that the extracts of the sintered Mg65–Zn30–Ca5 and Mg70–Zn25–Ca5 alloys did not induce cytotoxicity toward human fibroblast cells. The generation of biodegradable Mg65–Zn30–Ca5 and Mg70–Zn25–Ca5 alloys may decrease the cost of surgery and other complications during post-surgery operations. The results found from the cytotoxicity, corrosion, and mechanical tests recommend the need for more complementary tests, for example in vivo tests, given that they can reveal the effects that these alloys would have on an organism, which can pave the way for their use as temporary implants in clinical applications.

Author Contributions: Conceptualization, S.G. and A.M.; methodology, S.G., A.M. and J.S.-O.T.; formal analysis S.G., A.M., H.M. and E.V.V.; investigation, S.G., R.G., A.M. and J.S.-O.T.; writing-original draft preparation, S.G., A.M. and J.S.-O.T.; writing-review and editing, H.M. and E.V.V.; supervision, A.M.; Funding acquisition A.M. All authors have read and agreed to the published version of the manuscript.

Funding: This work was financed by CONACyT [Grant Number 467318].

Institutional Review Board Statement: Not applicable.

Informed Consent Statement: Not applicable.

Data Availability Statement: Not applicable.

Acknowledgments: CONACyT beca Posdoctoral.

Conflicts of Interest: The authors declare no conflict of interest.

References

1. Gu, X.; Zheng, Y.; Cheng, Y.; Zhong, S.; Xi, T. In vitro corrosion and biocompatibility of binary magnesium alloys. *Biomaterials* **2009**, *30*, 484–498. [[CrossRef](#)]
2. Witte, F.; Kaese, V.; Haferkamp, H.; Switzer, E.; Meyer-Lindenberg, A.; Wirth, C.J.; Windhagen, H. In vivo corrosion of four magnesium alloys and the associated bone response. *Biomaterials* **2005**, *26*, 3557–3563. [[CrossRef](#)] [[PubMed](#)]
3. Song, G. Control of biodegradation of biocompatible magnesium alloys. *Corros. Sci.* **2007**, *49*, 1696–1701. [[CrossRef](#)]
4. Staiger, M.P.; Pietak, A.M.; Huadmai, J.; Dias, G. Magnesium and its alloys as orthopedic biomaterials: A review. *Biomaterials* **2006**, *27*, 1728–1734. [[CrossRef](#)] [[PubMed](#)]
5. Saris, N.E.; Mervaala, E.; Karppanen, H.; Khawaja, J.A.; Lewenstam, A. Magnesium. An update on physiological, clinical and analytical aspects. *Clin. Chim. Acta* **2000**, *294*, 1–26. [[CrossRef](#)] [[PubMed](#)]

6. Wen, C.E.; Mabuchi, M.; Yamada, Y.; Shimojima, K.; Chino, Y.; Asahina, T. Processing of biocompatible porous Ti and Mg. *Scr. Mater.* **2001**, *45*, 1147–1153. [[CrossRef](#)]
7. Sun, Y.; Zhang, B.; Wang, Y.; Geng, L.; Jiao, X. Preparation and characterization of a new biomedical Mg–Zn–Ca alloy. *Mater. Des.* **2012**, *34*, 58–64. [[CrossRef](#)]
8. Shadanbaz, S.; Dias, G.J. Calcium phosphate coatings on magnesium alloys for biomedical applications: A review. *Acta Biomater.* **2012**, *8*, 20–30. [[CrossRef](#)]
9. Tapiero, H.; Tew, K.D. Trace elements in human physiology and pathology: Zinc and metallothioneins. *Biomed. Pharmacother.* **2003**, *57*, 399–411. [[CrossRef](#)]
10. Sandstead, H.H. Understanding zinc: Recent observations and interpretations. *J. Lab. Clin. Med.* **1994**, *124*, 322–327.
11. Prasad, A.S. Zinc: An overview. *Nutrition* **1995**, *11*, 93–99.
12. Schaafsma, A.; Beelen, G.M. Eggshell powder, a comparable or better source of calcium than purified calcium carbonate: Piglet studies. *J. Sci. Food Agric.* **1999**, *79*, 1596–1600. [[CrossRef](#)]
13. Brini, M.; Cali, T.; Ottolini, D.; Carafoli, E. Intracellular calcium homeostasis and signaling. *Met. Ions Life Sci.* **2013**, *12*, 119–168. [[CrossRef](#)] [[PubMed](#)]
14. Sigel, A.; Sigel, H.; Sigel, R.K.O. *Interrelations between Essential Metal Ions and Human Diseases*; Springer: Berlin/Heidelberg, Germany, 2013.
15. Li, Z.; Gu, X.; Lou, S.; Zheng, Y. The development of binary Mg–Ca alloys for use as biodegradable materials within bone. *Biomaterials* **2008**, *29*, 1329–1344. [[CrossRef](#)] [[PubMed](#)]
16. Velikokhatnyi, O.I.; Kumta, P.N. First-principles studies on alloying and simplified thermodynamic aqueous chemical stability of calcium-, zinc-, aluminum-, yttrium- and iron-doped magnesium alloys ☆. *Acta Biomater.* **2010**, *6*, 1698–1704. [[CrossRef](#)] [[PubMed](#)]
17. El-Rahman, S.S. Neuropathology of aluminum toxicity in rats (glutamate and GABA impairment). *Pharmacol. Res.* **2003**, *47*, 189–194. [[CrossRef](#)]
18. Hirano, S.; Suzuki, K.T. Exposure, metabolism, and toxicity of rare earths and related compounds. *Environ. Health Perspect.* **1996**, *104* (Suppl. S1), 85–95. [[CrossRef](#)] [[PubMed](#)]
19. Abbasi, M.; Sajjadi, S.A.; Azadbeh, M. An investigation on the variations occurring during Ni₃Al powder formation by mechanical alloying technique. *J. Alloys Compd.* **2010**, *497*, 171–175. [[CrossRef](#)]
20. Neves, F.; Fernandes, F.M.B.; Martins, I.; Correia, J.B. Parametric optimization of Ti–Ni powder mixtures produced by mechanical alloying. *J. Alloys Compd.* **2011**, *509*, S271–S274. [[CrossRef](#)]
21. Matias, T.; Roche, V.; Nogueira, R.; Asato, G.; Kiminami, C.; Bolfarini, C.; Jorge, A. MG–Zn–CA Amorphous Alloys for application as temporary implant: Effect of zn content on the mechanical and corrosion properties. *Mater. Des.* **2016**, *110*, 188–195. [[CrossRef](#)]
22. Gu, X.; Zheng, Y.; Zhong, S.; Xi, T.; Wang, J.; Wang, W. Corrosion of, and cellular responses to Mg–Zn–Ca Bulk Metallic Glasses. *Biomaterials* **2010**, *31*, 1093–1103. [[CrossRef](#)]
23. González, S.; Pellicer, E.; Fornell, J.; Blanquer, A.; Barrios, L.; Ibáñez, E.; Sort, J. Improved mechanical performance and delayed corrosion phenomena in biodegradable Mg–Zn–Ca alloys through pd-alloying. *J. Mech. Behav. Biomed. Mater.* **2012**, *6*, 53–62. [[CrossRef](#)] [[PubMed](#)]
24. Campos Becerra, L.H.; Hernández Rodríguez, M.A.; Esquivel Solís, H.; Lesso Arroyo, R.; Torres Castro, A. Bio-inspired biomaterial mg–zn–ca: A review of the main mechanical and biological properties of MG-based alloys. *Biomed. Phys. Eng. Express* **2020**, *6*, 042001. [[CrossRef](#)] [[PubMed](#)]
25. Gonzaga, S.R.; Sedano, A.; Colín, J.M.; Torres-Islas, A.; Molina-Ocampo, A. Production of biodegradable Mg-based alloys by mechanical alloying. *Dig. J. Nanomater. Biostructures* **2021**, *16*, 1537–1545.
26. *ISO 10993–12 2012*; Biological Evaluation of Medical Devices, Part 12: Sample Preparation and Reference Materials. ISO: Geneva, Switzerland, 2012.
27. Skehan, P.; Storeng, R.; Scudiero, D.; Monks, A.; McMahon, J.; Vistica, D.; Boyd, M.R. New colorimetric cytotoxicity assay for anticancer-drug screening. *JNCI J. Natl. Cancer Inst.* **1990**, *82*, 1107–1112. [[CrossRef](#)] [[PubMed](#)]
28. Savale, S.K. Sulforhodamine B (SRB) Assay of curcumin loaded nanoemulsion by using glioblastoma cell line. *Asian J. Biomater. Res.* **2017**, *3*, 26–30.
29. Orellana, E.; Kasinski, A. Sulforhodamine B (SRB) assay in cell culture to investigate cell proliferation. *Bioprotocol* **2016**, *6*, e1984. [[CrossRef](#)]
30. Paula, A.; Laranjo, M.; Marto, C.M.; Abrantes, A.M.; Casalta-Lopes, J.; Gonçalves, A.C.; Carrilho, E. Biodentine™ Boosts, whiteproroot® MTA increases and Life® suppresses odontoblast activity. *Materials* **2019**, *12*, 1184. [[CrossRef](#)]
31. Kazak, M.; Donmez, N.; Bahadori, F.; Betul, Y.V.; Kocyigit, A. A preliminary research study on the cytotoxicity of expired and non-expired composite resins: In vitro study. *Odovtos-Int. J. Dent. Sci.* **2020**, *22*, 123–134. [[CrossRef](#)]
32. Suryanarayana, C. Mechanical alloying: A novel technique to synthesize Advanced Materials. *Research* **2019**, *2019*, 4219812. [[CrossRef](#)]
33. Abdoli, H.; Farnoush, H.; Salahi, E.; Pourazrang, K. Study of the densification of a nanostructured composite powder: Part 1: Effect. *Mater. Sci. Eng.* **2008**, *486*, 580–584. [[CrossRef](#)]
34. Jang, J.S.C.; Koch, C.C. Amorphization and disordering of the Ni₃Al ordered intermetallic by mechanical milling. *J. Mater. Res.* **1990**, *5*, 498–510. [[CrossRef](#)]

35. Suryanarayana, C.; Korth, G.E.; Chen, G.-H.; Frefer, A.; Froes, F.H. Thermal stability of nanostructured titanium aluminides. *Nanostruct. Mater.* **1993**, *2*, 527–535. [[CrossRef](#)]
36. Zartner, P.; Cesnjevar, R.; Singer, H.; Weyand, M. First successful implantation of a biodegradable metal stent into the left pulmonary artery of a preterm baby. *Catheter. Cardiovasc. Interv.* **2005**, *66*, 590–594. [[CrossRef](#)]
37. Erbel, R.; Di Mario, C.; Bartunek, J.; Bonnier, J.; de Bruyne, B.; Eberli, F.R.; Erne, P.; Haude, M.; Heublein, B.; Horrigan, M.; et al. Temporary scaffolding of coronary arteries with bioabsorbable magnesium stents: A prospective, non-randomised multicentre trial. *Lancet* **2007**, *369*, 1869–1875. [[CrossRef](#)]
38. Goodship, A.E. AO principles of fracture management (book and CD-ROM). *J. Bone Jt. Surg.* **2001**, *83-B*, 933–934. [[CrossRef](#)]
39. ASTM Standard G102-89; Standard Practice for Calculation of Corrosion Rates and Related Information from Electrochemical. ASTM International: West Conshohocken, PE, USA, 2015.
40. Salleh, E.M.; Zuhailawati, H.; Mohd Noor, S.N.F.; Othman, N.K. In vitro biodegradation and mechanical properties of Mg-Zn alloy and Mg-Zn-hydroxyapatite composite Produced by Mechanical Alloying for Potential Application in Bone Repair. *Metall. Mater. Trans. A* **2018**, *49*, 5888–5903. [[CrossRef](#)]
41. Witte, F.; Hort, N.; Vogt, C.; Cohen, S.; Kainer, K.U.; Willumeit, R.; Feyerabend, F. Degradable biomaterials based on magnesium corrosion. *Curr. Opin. Solid State Mater. Sci.* **2008**, *12*, 63–72. [[CrossRef](#)]
42. Xu, L.; Yu, G.; Zhang, E.; Pan, F.; Yang, K. In vivo corrosion behavior of Mg-Mn-Zn alloy for bone implant application. *J. Biomed. Mater. Res. Part A* **2007**, *83*, 703–711. [[CrossRef](#)]
43. Wang, H.; Estrin, Y.; Zúberová, Z. Bio-corrosion of a magnesium alloy with different processing histories. *Mater. Lett.* **2008**, *62*, 2476–2479. [[CrossRef](#)]
44. Suryanarayana, C.; Ivanov, E.; Boldyrev, V.V. The science and technology of mechanical alloying. *Mater. Sci. Eng.* **2001**, *304–306*, 151–158. [[CrossRef](#)]
45. Cipriano, A.F.; Zhao, T.; Johnson, I.; Guan, R.G.; Garcia, S.; Liu, H. In vitro degradation of four magnesium–zinc–strontium alloys and their cytocompatibility with human embryonic stem cells. *J. Mater. Sci. Mater. Med.* **2013**, *24*, 989–1003. [[CrossRef](#)] [[PubMed](#)]
46. Witte, F. The history of biodegradable magnesium implants: A review. *Acta Biomater.* **2010**, *6*, 1680–1692. [[CrossRef](#)] [[PubMed](#)]

Disclaimer/Publisher’s Note: The statements, opinions and data contained in all publications are solely those of the individual author(s) and contributor(s) and not of MDPI and/or the editor(s). MDPI and/or the editor(s) disclaim responsibility for any injury to people or property resulting from any ideas, methods, instructions or products referred to in the content.